Investigation of Growth Mechanisms of Clusters in a Silane Discharge With the Use of a Fluid Model

Kathleen De Bleecker, Annemie Bogaerts, Wim Goedheer, and Renaat Gijbels

***Abstract*—A one-dimensional fluid model was developed to study the formation of dust nanoparticles in a low-pressure capacitively coupled radio-frequency silane (SiH_4) discharge. In this model, the particle balances, the electron energy balance, and the Poisson equation are solved self-consistently. A set of 66 species, including neutrals, radicals, ions, and electrons, are incorporated. A total of 111 reactions are described in the model, comprising electron impact reactions with silanes, neutral-neutral, and ion-neutral reactions. Plasma conditions are typically those used for the deposition of amorphous silicon (a-Si:H). The model includes the formation of silicon hydrides (Si_nH_m) containing up to 12 silicon atoms. Anion-induced chain reactions are considered to be the main pathway leading to cluster formation.**

***Index Terms*—Dusty silane plasma, nucleation.**

I. INTRODUCTION

PARTICLE formation in low-pressure silane discharges, creating "dusty" plasmas, has gained substantial interest over the past years [1]–[4]. Indeed, the presence of dust in industrial plasma reactors can lead to the production of defective films if the particles are incorporated into the film during the plasma-enhanced chemical vapor deposition (PECVD) process [5], [6]. On the other hand, solar cell application seems to benefit from the presence of nanometer-size particles in the amorphous silicon layer (a-Si:H), as an increase in the performance of the solar cell is observed [7], [8]. Hence, understanding the origin and the behavior of these particles can help in finding efficient ways to minimize, or to eliminate, undesirable particles in the microelectronics, as well as enhance the embedded particles to improve film properties. Comprehension of these aspects advances the development of both fundamental knowledge and potential applications.

Here, we study the initial mechanism by which silicon particles start growing, which is experimentally the most difficult stage to observe due to the very small size of the particles ($r_p <$ 5 nm) requiring sophisticated diagnostics [9]. Therefore, theoretical models can provide an alternative. Investigations [5], [10] have shown that particles are formed due to successive reactions in the gas phase, known as gas phase polymerization, and the surface is not believed to play any role in the production process. Negative ions are generally considered to be the particle precursors, since they are trapped in the plasma bulk and have a longer residence time in the plasma [11]–[13]. Reactions with negative ions are therefore considered as the primary clustering pathway in our simulations.

A description of the model, including the plasma kinetics, is presented in Section II. In Section III, results of the various simulations are represented and discussed. Finally, the conclusion is given in Section IV.

Manuscript received August 19, 2003; revised November 5, 2003. This work was supported by the Institute for the Promotion of Innovation through Science and Technology in Flanders (IWT-Vlaanderen), by the Flemish Fund for Scientific research (FWO), and by the IUAP-V project.

K. De Bleecker, A. Bogaerts, and R. Gijbels are with the Department of Chemistry, University of Antwerp, 2610 Wilrijk, Belgium (e-mail: kathleen.debleecker@ua.ac.be).

W. Goedheer is with the FOM-Institute for Plasma Physics "Rijnhuizen" 3430 BE Nieuwegein, The Netherlands.

Digital Object Identifier 10.1109/TPS.2004.826095

II. MODEL DESCRIPTION

A. Fluid Model

The model for describing the nucleation of dust in silane plasmas is based on the fluid model developed by Nienhuis *et al.* [14] for the description of a silane/hydrogen discharge.

This fluid model describes the discharge by a combination of particle, momentum, and energy density balances of the ions, electrons, and neutrals. The balance equations are coupled to the Poisson equation for the calculation of the electric field. Typical discharge quantities such as the electric field, densities, and fluxes of the particles as a function of space and time are calculated self-consistently. An overview of the model can be found elsewhere [14], [15]. The system of nonlinear differential equations is solved numerically. For the spatial discretization of the balance equations, the Scharfetter–Gummel exponential scheme is used [16]. The computational grid is equidistant and contains 64 grid points. An implicit second-order method [17] is applied to numerically treat the time evolution of the balance equations. Finally, the Newton–Raphson method is used to solve the resulting set of nonlinear equations. Convergence of the fluid model is reached when the relative changes of the discharge parameters between two succeeding radio-frequency (RF) cycles are less than 10^{-6}. Further details concerning the numerical techniques and algorithms can be found in [17] and [18].

No secondary electrons are taken into account, so the results are limited to the α-regime of a capacitively coupled RF discharge. This is a good estimate since the results are computed at low pressures (order of several hundred mtorr) and power (5 W) where the RF discharge is assumed to operate in the alfa regime [19], [20]. Power input into the plasma is transferred to the charged species (electrons and ions) by ohmic heating.

B. Plasma Kinetics

A basic set of reactions has been taken from Nienhuis *et al.* [14] for a silane discharge without the inclusion of nanoparticles. A series of chemical reactions has been gradually incor-

0093-3813/04$20.00 © 2004 IEEE

TABLE I
DIFFERENT SPECIES TAKEN INTO ACCOUNT IN THE MODEL, BESIDES THE ELECTRONS

Molecules	Ions	Radicals
SiH_4	SiH_3^+, $Si_2H_4^+$, SiH_3^-, SiH_2^-	SiH_3, SiH_2
H_2	H_2^+	H
Si_2H_6, Si_3H_8, Si_4H_{10}, Si_5H_{12}	$Si_2H_5^-$, $Si_3H_7^-$, $Si_4H_9^-$, $Si_5H_{11}^-$	Si_2H_5, Si_3H_7, Si_4H_9, Si_5H_{11}
Si_6H_{14}, Si_7H_{16}, Si_8H_{18}, Si_9H_{20}	$Si_6H_{13}^-$, $Si_7H_{15}^-$, $Si_8H_{17}^-$, $Si_9H_{19}^-$	Si_6H_{13}, Si_7H_{15}, Si_8H_{17}, Si_9H_{19}
$Si_{10}H_{22}$, $Si_{11}H_{24}$, $Si_{12}H_{26}$	$Si_{10}H_{21}^-$, $Si_{11}H_{23}^-$, $Si_{12}H_{25}^-$	$Si_{10}H_{21}$, $Si_{11}H_{23}$, $Si_{12}H_{25}$
	$Si_2H_4^-$, $Si_3H_6^-$, $Si_4H_8^-$, $Si_5H_{10}^-$	Si_2H_4, Si_3H_6, Si_4H_8, Si_5H_{10}
	$Si_6H_{12}^-$, $Si_7H_{14}^-$, $Si_8H_{16}^-$, $Si_9H_{18}^-$	Si_6H_{12}, Si_7H_{14}, Si_8H_{16}, Si_9H_{18}
	$Si_{10}H_{20}^-$, $Si_{11}H_{22}^-$, $Si_{12}H_{24}^-$	$Si_{10}H_{20}$, $Si_{11}H_{22}$, $Si_{12}H_{24}$

TABLE II
ELECTRON IMPACT COLLISIONS USED IN THE MODEL

	Reaction	Reaction type	Reference
1.	$SiH_4 + e^- \rightarrow SiH_3^+ + H + 2e^-$	dissociative ionization	[22]
2.	$Si_2H_6 + e^- \rightarrow Si_2H_4^+ + 2H + 2e^-$	dissociative ionization	[22]
3.	$SiH_4^{(0)} + e^- \rightarrow SiH_4^{(2-4)} + e^- \rightarrow SiH_4^{(0)} + e^-$	vibrational excitation	[23]
4.	$SiH_4^{(0)} + e^- \rightarrow SiH_4^{(1-3)} + e^- \rightarrow SiH_4^{(0)} + e^-$	vibrational excitation	[23]
5.	$SiH_4 + e^- \rightarrow SiH_3 + H + e^-$	dissociation	[24], [25]
6.	$SiH_4 + e^- \rightarrow SiH_2 + 2H + e^-$	dissociation	[24], [25]
7.	$Si_2H_6 + e^- \rightarrow SiH_3 + SiH_2 + H + e^-$	dissociation	[24]
8.	$SiH_4 + e^- \rightarrow SiH_3^- + H$	dissociative attachment	[26]
9.	$SiH_4 + e^- \rightarrow SiH_2^- + 2H$	dissociative attachment	[26]
10.	$H_2 + e^- \rightarrow H_2^+ + 2e^-$	ionization	[27]
11.	$H_2 + e^- \rightarrow H_2^{(v=1)} + e^-$	vibrational excitation	[28]
12.	$H_2 + e^- \rightarrow H_2^{(v=2)} + e^-$	vibrational excitation	[28]
13.	$H_2 + e^- \rightarrow H_2^{(v=3)} + e^-$	vibrational excitation	[28]
14.	$H_2 + e^- \rightarrow H + H + e^-$	dissociation	[29]

porated, starting from silane leading to the formation of larger silicon hydrides, mostly through the anion pathway. Silicon hydrides containing up to 12 silicon atoms are included. A sensitivity study has been performed in order to obtain a minimum set of different species and reactions, which still gives a reasonable picture of the growth process. When a species or reaction has a negligible influence on the overall plasma chemistry, it is removed from the calculations. Examples are given below.

Table I gives an overview of the different species considered in our model, besides the electrons. The inlet gas SiH_4 will of course play an important role in the plasma and will be present at the highest density. Vibrationally excited silane species are not represented by separate species in this model, in order to reduce the computational effort. Electron reactions leading to vibrational excitation are, however, included, where the vibrationally excited molecules are treated as ground state molecules, thus not requiring their separate incorporation (see Table II). Higher order silanes (Si_nH_{2n+2}), especially disilane, are incorporated, as they take part in the cluster formation and are present at relatively high densities. If a species Si_nH_{2n+2} is included, then it is also necessary to include the radical Si_nH_{2n+1}, since the H abstraction reactions are considered to be important (see Table III). In addition to the silanes, the silylenes (Si_nH_{2n}) have to be incorporated, mainly because their corresponding anions represent a possible clustering route. Silylenes are isomers of silenes (i.e., molecules with a double bond between two silicon atoms) but with a single bond between the two silicon atoms and with two nonbonding electrons. They are considered to be reactive, thus we classify them as radicals. Although silylenes can isomerize to silenes, which are thermodynamically more stable, the silenes are not considered in our model, because they are chemically inactive and will only accumulate in the reactor at relatively low densities. Silyl anions ($Si_nH_{2n+1}^-$) and silylene anions ($Si_nH_{2n}^-$) up to 12 silicon atoms are also taken into account, because the growth of clusters occurs mainly through the anion pathway [12], [21] making them the most prominent particles to include in the simulations. No distinction was made between linear and cyclic molecules.

Table II outlines the electron reactions taken into account. The rate constants of the electron-induced reactions depend strongly on the electron energy distribution function, which is obtained from the two-term expansion of the Boltzmann equation. Rate coefficients as a function of the average electron energy are introduced into the fluid model. The references for the cross section data for the ionization, dissociation, attachment, and vibrational excitation of silane, and in some cases of disilane and hydrogen, are indicated in Table II. Dissociation of silane leads mostly to SiH_3 and SiH_2 radicals with a branching ratio of 0.17/0.83 for SiH_3/SiH_2 [24]. Although ionization can lead to a number of positive ions, the ionization cross sections of Si_2H_6, SiH_4, and H_2 have been lumped and attached to the ion which is most likely formed, i.e., $Si_2H_4^+$, SiH_3^+, and H_2^+, respectively. For dissociative attachment of SiH_4, a similar procedure has been used. Only SiH_3^- and SiH_2^- are considered to be the most abundant anions formed by dissociative attachment of SiH_4, with over 70% leading to the formation of SiH_3^-.

TABLE III
CHEMICAL REACTIONS TAKEN INTO ACCOUNT IN THE MODEL

	Reaction	Rate constant ($m^3\ s^{-1}$)	Comment		Ref.
Hydrogen abstraction					
1.	$SiH_4 + H \rightarrow SiH_3 + H_2$	1.2×10^{-18}	$2.8 \times 10^{-17} \exp(-1250/T_{gas})$		[36], [37]
2.	$Si_2H_6 + H \rightarrow Si_2H_5 + H_2$	7.0×10^{-18}	$1.6 \times 10^{-16} \exp(-1250/T_{gas})$		[36], [37]
3.	$Si_2H_6 + H \rightarrow SiH_3 + SiH_4$	3.5×10^{-18}	$0.8 \times 10^{-16} \exp(-1250/T_{gas})$		[36], [37]
4.	$Si_nH_{2n+2} + H \rightarrow Si_nH_{2n+1} + H_2$	1.1×10^{-17}	$2.4 \times 10^{-16} \exp(-1250/T_{gas})$	n=3,...,12	[36], est.
Cluster growth through SiH_2 insertion					
5.	$SiH_2 + H_2 \rightarrow SiH_4$	2.7×10^{-20}	$3.0 \times 10^{-18} [1 - (1 + 2.3 \times 10^{-4}\ p_0)^{-1}]$		[36]
6.	$SiH_2 + SiH_4 \rightarrow Si_2H_6$	2.3×10^{-17}	$2.0 \times 10^{-16} [1 - (1 + 0.0032\ p_0)^{-1}]$		[36]
7.	$SiH_2 + Si_nH_{2n+2} \rightarrow Si_{n+1}H_{2n+4}$	4.9×10^{-17}	$4.2 \times 10^{-16} [1 - (1 + 0.0033\ p_0)^{-1}]$	n=2,...,11	[36]
Other neutral-neutral reactions					
8.	$Si_2H_5 + Si_2H_5 \rightarrow Si_4H_{10}$	1.5×10^{-16}			[36], est.
9.	$SiH_3 + SiH_3 \rightarrow SiH_2 + SiH_4$	1.5×10^{-16}			[36], [38]
Cluster growth through silyl anions ($Si_nH_{2n+1}^-$) with silane					
10.	$Si_nH_{2n+1}^- + SiH_4 \rightarrow Si_{n+1}H_{2n+3}^- + H_2$	$\sim 10^{-16}$	Langevin $\times$ 0.1	n=1,...,11	[33]
Cluster growth through silylene anions ($Si_nH_{2n}^-$) with silane					
11.	$Si_nH_{2n}^- + SiH_4 \rightarrow Si_{n+1}H_{2n+2}^- + H_2$	$\sim 10^{-16}$	Langevin $\times$ 0.1	n=1,...,11	[33]
Neutralization reactions of silyl anions with SiH_3^+ and $Si_2H_4^+$					
12.	$Si_nH_{2n+1}^- + SiH_3^+ \rightarrow Si_nH_{2n+1} + SiH_3$	$\sim 10^{-14}$	calc.	n=1,...,12	[39]
13.	$Si_nH_{2n+1}^- + Si_2H_4^+ \rightarrow Si_nH_{2n+1} + 2\ SiH_2$	$\sim 10^{-14}$	calc.	n=1,...,12	[39]
Neutralization reactions of silylene anions with SiH_3^+ and $Si_2H_4^+$					
14.	$Si_nH_{2n}^- + SiH_3^+ \rightarrow Si_nH_{2n} + SiH_3$	$\sim 10^{-14}$	calc.	n=1,...,12	[39]
15.	$Si_nH_{2n}^- + Si_2H_4^+ \rightarrow Si_nH_{2n} + 2\ SiH_2$	$\sim 10^{-14}$	calc.	n=1,...,12	[39]

Indeed, the cross sections for the production of SiH^- are too low [26], and SiH^- is therefore not considered as a separate species. The partial cross sections of SiH_3^- and SiH_2^- are obtained from [26]. These cross sections are two orders of magnitude smaller than the corresponding dissociative ionization cross sections, but this process represents the most important source of negative ions in the silane plasma. Dissociative attachment cross sections of Si_2H_6 and H_2 can be found in [30] and [31], respectively. However, since the density of Si_2H_6 is more than one order of magnitude lower than the density of SiH_4 (see below), the dissociative attachment to Si_2H_6 is neglected. Although, the rate of electron attachment increases strongly with particle size [32], no electron attachment to larger silicon hydrides is included, since the much lower densities of larger silicon hydrides in comparison to silane makes these attachments less important. Moreover, for particles smaller than 2 nm, the time needed for an electron to attach is much longer than the residence time of the particle in the plasma [32], so there is no possibility for these particles to become charged. H^- is not included either, because it appears to have a negligible influence on the plasma chemistry [14].

Table III summarizes the chemical reactions (neutral-neutral reactions and ion-neutral reactions) which are included in our model. The reaction rate coefficients are assumed to be constant. Because some rates are a function of gas temperature or background pressure, their general notation is also given (see the comment column of the table). The values used in our model are calculated for a gas pressure of 0.3 torr or 40 Pa (p_0 is denoted in Pascal units in Table III) and a gas temperature of 400 K. We consider reactions between silicon hydrides containing up to 12 silicon atoms. An extensive overview is given by Bhandarkar *et al.* [33] and has been utilized to investigate which reactions can be considered as important. The rate constants for larger silicon hydrides in the model of Bhandarkar are based on the calculations made by Girshick and coworkers [33], [34]. Based on the known reactivity and thermochemistry of smaller silicon hydrides, they estimated the thermochemistry and kinetics of larger silicon species. By using a group additivity scheme, the thermodynamic properties of arbitrary silicon hydride clusters could be approximated [34], [35].

The reactions can be subdivided into: 1) H abstraction (reactions 1–4 in Table III); 2) SiH_2 insertion leading to the formation of larger silanes (reactions 5–7); 3) other neutral-neutral reactions (reactions 8–9); 4) anion-neutral (reactions 10–11); and 5) mutual neutralization reactions (reactions 12–15).

1) Reactions Involving Neutrals: A basic set of reactions used to describe a "regular" silane/hydrogen discharge (i.e., without dust formation) has been taken from Nienhuis *et al.* [14] (reactions 1–9, Table III). The rate coefficients of $SiH_2 + Si_nH_{2n+2} \rightarrow Si_{n+1}H_{2n+4}, n \geq 3$ are assumed to be equal to that of $SiH_2 + Si_2H_6 \rightarrow Si_3H_8$ [14]. Chemical reactions of positive ions with background neutrals, e.g., $H_2^+ + SiH_4 \rightarrow SiH_3^+ + H_2 + H$ or $SiH_2^+ + SiH_4 \rightarrow SiH_3^+ + SiH_3$, have not been included, since they have no influence on the further growth of the clusters. Furthermore, in [14] it is stated that, although the rate coefficients of these reactions are of

equal magnitude as some radical-neutral reactions, the densities of the ions are much lower than the radical densities (see below), making ion-neutral reactions of negligible influence on the densities of the background gases (i.e., SiH_4, Si_2H_6, and H_2). Also, the addition between two radicals to form a higher silane is limited to $Si_2H_5 + Si_2H_5 \rightarrow Si_4H_{10}$. Furthermore, $SiH_3 + SiH_3$ can lead to either Si_2H_6 or $SiH_2 + SiH_4$. However, only the latter reaction is included, since Si_2H_6 is likely to dissociate in SiH_2 and SiH_4 [36]. For completeness, we have also explored other possible reactions between two silyl radicals using the same rate constant as in reactions 8–9 of Table III (i.e., 1.5×10^{-16} $m^3 \cdot s^{-1}$). This included reactions such as $Si_3H_7 + SiH_3 \rightarrow Si_4H_{10}$. Adding such reactions to the mechanism generally had no effect on the growth of the species, since our calculations showed that the densities of higher silane radicals are too low to make these reactions effective.

Chemically activated channels for disilane and trisilane decomposition are not incorporated, e.g.,

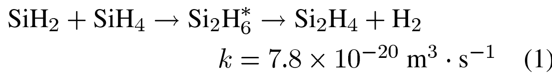

$$SiH_2 + SiH_4 \rightarrow Si_2H_6^* \rightarrow Si_2H_4 + H_2 \qquad k = 7.8 \times 10^{-20}\ m^3 \cdot s^{-1} \quad (1)$$

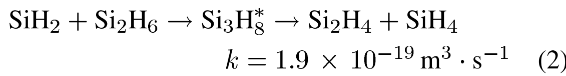

$$SiH_2 + Si_2H_6 \rightarrow Si_3H_8^* \rightarrow Si_2H_4 + SiH_4 \qquad k = 1.9 \times 10^{-19}\ m^3 \cdot s^{-1} \quad (2)$$

mainly because they do not have an effect on the further cluster growth. Although the above reactions yield a rise in the density of Si_2H_4, we do not take them into account. Indeed, as stated above, the silylenes are only incorporated in our model because their anions are considered to be important, and they form the neutral silylenes by neutralization reactions (see below).

2) Reactions Involving Anions: Anions are formed by the attachment of electrons to SiH_4 creating SiH_3^- and SiH_2^-. Starting from either SiH_3^- or SiH_2^-, two separate reaction chains lead to the formation of larger negative clusters by anion-neutral reactions. The SiH_3^- ion has a filled valence shell and can slowly cluster with silane

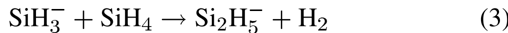

$$SiH_3^- + SiH_4 \rightarrow Si_2H_5^- + H_2 \quad (3)$$

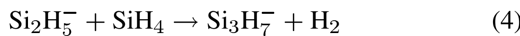

$$Si_2H_5^- + SiH_4 \rightarrow Si_3H_7^- + H_2 \quad (4)$$

$$\vdots$$

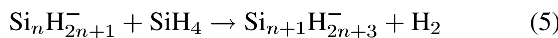

$$Si_nH_{2n+1}^- + SiH_4 \rightarrow Si_{n+1}H_{2n+3}^- + H_2 \quad (5)$$

forming larger silyl anions.

A second important chain of anion-neutral reactions starts from SiH_2^-

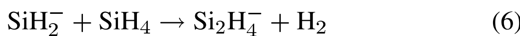

$$SiH_2^- + SiH_4 \rightarrow Si_2H_4^- + H_2 \quad (6)$$

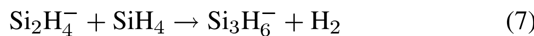

$$Si_2H_4^- + SiH_4 \rightarrow Si_3H_6^- + H_2 \quad (7)$$

$$\vdots$$

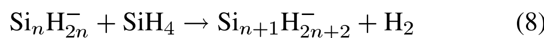

$$Si_nH_{2n}^- + SiH_4 \rightarrow Si_{n+1}H_{2n+2}^- + H_2 \quad (8)$$

leading to larger silylene anions.

Exact data for the rate constants of these anion-neutral reactions are not known. A theoretical upper limit for anion–molecule collision rates is given by the Langevin rate constants. Since Langevin rates are known to overestimate the actual rates, they are reduced according to [33] by an order of magnitude. The following formula is used to calculate the Langevin rate constants k_L [36]:

$$k_L = e\left(\frac{\pi}{\epsilon_0}\right)^{1/2}\left(\frac{\alpha}{m_r}\right)^{1/2} \quad (9)$$

where α represents the polarizability of the neutral atom or molecule (in $Å^3$) and m_r is the reduced mass (in amu) of the two reacting species. For higher order silicon molecules, a scaling law is used to obtain their polarizability [36]

$$\alpha(Si_nH_{2n+1}) \approx \alpha(SiH_4)[1 + 0.8(n-1)] = 4.62(0.2 + 0.8n)\ (Å^3) \quad (10)$$

where 4.62 ($Å^3$) represents the polarizability of SiH_4. Hence, the polarizability essentially scales with the number of silicon atoms present in the molecule.

The anion-neutral reactions proceed all at nearly the same reaction rate (about 10^{-16} $m^3 \cdot s^{-1}$, as depicted in Table III). More specifically, the rate slightly decreases from 1.3×10^{-16} $m^3 \cdot s^{-1}$ for $SiH_m^- + SiH_4 \rightarrow Si_2H_{m+2}^- + H_2$ ($m = 2$ or 3) to 9.3×10^{-17} $m^3 \cdot s^{-1}$, for $Si_{11}H_m^- + SiH_4 \rightarrow Si_{12}H_{m+2}^- + H_2$ ($m = 22$ or 23). Although in [33] two kinetic bottlenecks in the anion-radical clustering chain are incorporated, we do not take them into account. Indeed, Bhandarkar *et al.* assumed that the reactions $Si_4H_9^- + SiH_4 \rightarrow Si_5H_{11}^- + H_2$ and $Si_7H_{15}^- + SiH_4 \rightarrow Si_8H_{17}^- + H_2$ are energetically unfavorable, because they lead to a positive change in Gibbs free energy (ΔG) of respectively 7 kcal mol^{-1} and 9.4 kcal mol^{-1}, whereas the other reactions in the same chain lead to a negative change in the Gibbs free energy [23]. However, since the calculation of the equilibrium constant depends on the thermochemical properties of the reactants and products, which are based on estimations, these bottlenecks might be artificial [40]. Moreover, vibrationally excited silanes may play an important role in the clustering process; hence, these bottlenecks will be eliminated due to the reaction with molecules carrying sufficient internal energy.

Similar to the anion-silane reactions described above, anions can also react with larger silicon hydrides (Si_nH_{2n+2} with $n > 1$), e.g., $SiH_3^- + Si_2H_6 \rightarrow Si_3H_7^- + H_2$ or $SiH_2^- + Si_3H_8 \rightarrow Si_4H_8^- + H_2$. However, these reactions are not taken into account, because they are nearly two orders of magnitude slower than the chains mentioned above, due to the lower concentrations of Si_2H_6 and especially of the higher order silanes.

In a later stage, we will include the effect of gas temperature on the cluster growth, since it has been experimentally observed that a temperature increase delays the dust formation induction period [32], [41].

It is worth mentioning that even modest production rates of anions can lead to substantial anion densities, because the ambipolar sheath field prevents them from reaching the reactor walls. The loss processes for silyl and silylene anions must therefore occur in the gas phase.

The most important loss process that must be considered is the mutual ion-ion neutralization,

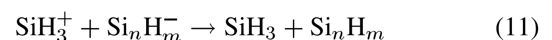

$$SiH_3^+ + Si_nH_m^- \rightarrow SiH_3 + Si_nH_m \quad (11)$$

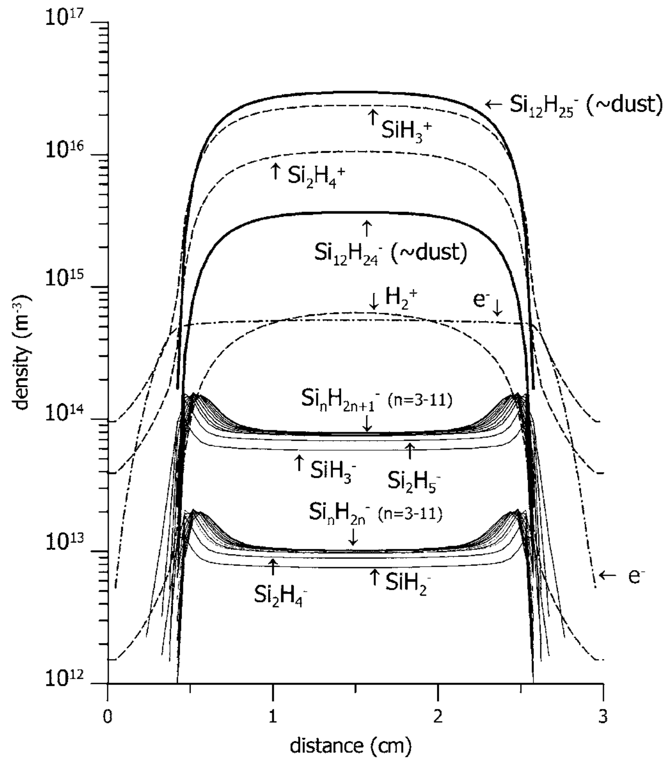

Fig. 1. Density profiles of the ions and electrons at a pressure of 0.3 torr, 5 W, 50 MHz, and 20 sccm inlet silane.

and

$$Si_2H_4^+ + Si_nH_m^- \rightarrow 2\ SiH_2 + Si_nH_m \tag{12}$$

where $m = 2n + 1$ for silyl anions (reactions 12–13, Table III) and $m = 2n$ for silylene anions (reactions 14–15 in Table III), respectively. Neutralization of the silyl and silylene anions occurs mainly through reaction with SiH_3^+, but reactions with $Si_2H_4^+$ are not completely negligible. Although another positive ion, H_2^+, is taken into account in the model, our calculations show that its density is too low to take any significant part in the neutralization process. The rate constants for mutual neutralization between cation i and anion j are calculated from the semiempirical formula derived by Hickman for gaseous cluster ions [39]

$$k_N \approx 5.34 \times 10^{-13} \times \left(\frac{T_{\text{gas}}}{300}\right)^{-0.5} \times m_r^{-0.5} \times \text{EA}_j^{-0.4}\ (\text{m}^3 \cdot \text{s}^{-1}) \tag{13}$$

with the gas temperature T_{gas} in kelvin, the reduced mass m_r in amu, and the electron affinity EA_j in electronvolts (eV). The corresponding electron affinities are taken from [33].

Alternatively, the reactants can also recombine to a larger neutral cluster

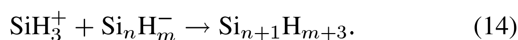

$$SiH_3^+ + Si_nH_m^- \rightarrow Si_{n+1}H_{m+3}. \tag{14}$$

However, our calculations show that assuming either neutralization or recombination with the same reaction rate coefficients does not make any difference for the plasma chemistry and the cluster growth. Therefore, we have adopted mutual neutralization instead of recombination, because it requires the introduction of fewer species in the model.

Electron detachment of the negative ions could be another loss process for the negative ions, but it is considered to be negligible in the present study. Furthermore, charge exchange between anions and silyl radicals, e.g., $Si_nH_m^- + Si_nH_{2n+1} \rightarrow Si_nH_m + Si_nH_{2n+1}^-$, has been neglected, since the densities of the various radicals are too low, even if these reactions are also calculated using the Langevin rate constants.

III. Results and Discussion

The calculations were carried out for a parallel-plate, capacitively coupled RF discharge, for a total pressure of 0.3 torr and a silane gas flow of 20 sccm. The electrode gap is set at 3 cm. Other plasma process parameters include a driving frequency of 50 MHz, a power of 5 W, and a gas temperature of 400 K. These are typical conditions for which cluster formation takes place. The time step is set at 2.5×10^{-10} s and a uniform simulation grid is used.

Typical results of this model are the density profiles and fluxes of the various species, as well as the distribution of the electric field and potential. In this paper, we focus our attention on the densities as a function of distance from the electrodes, which can give us an insight in the clustering process, e.g., which kind of anions are the most important.

The calculated density profiles for the different species listed in Table I are shown in Figs. 1–3 at 0.3 torr, 5 W, 50 MHz, and 20 sccm SiH_4. The electron density is plotted together with the ions in Fig. 1. To emphasize their different behavior, the neutrals, radicals, and ions have been plotted in separate figures.

In Fig. 1, the calculated densities of the ions are shown. A slight time variation of the ion profile will occur in the plasma sheaths; therefore, time-averaged densities of the ions are plotted. The positive ions are represented by a dashed line. The simulation results show that the dominant positive ion is SiH_3^+ with a density of 2×10^{16} m^{-3} in the plasma bulk, which is two times more than the density of $Si_2H_4^+$. Both species densities exceed the density of H_2^+ by almost two orders of magnitude. Therefore, ion-ion recombination reactions with H_2^+ do not have to be included in the model (see above).

All negative ions are confined to the bulk of the plasma and are almost absent in the sheaths. Silyl and silylene anions from $n = 3$ to $n = 11$, where n represents the number of silicon atoms, reach approximately equal concentrations, especially in the plasma center, and are indicated by the notation $Si_nH_{2n+1}^-$ and $Si_nH_{2n}^-$, respectively. The density profiles of the anions in both pathways appear to slightly increase with increasing n. This can be explained by the fact that in our model assumption we have used reduced Langevin rate constants for the anion-neutral reactions, which gradually decreases for larger anions due to an increase of the reduced mass [see (9)], leading to a slower reduction of the anion density. Moreover, for higher order anions, the anion-cation neutralization loss process diminishes, as the reaction rate also gradually decreases with increasing n [see (13)].

The two main anion clustering pathways are based on silyl and silylene anions. Therefore, the most prominent species

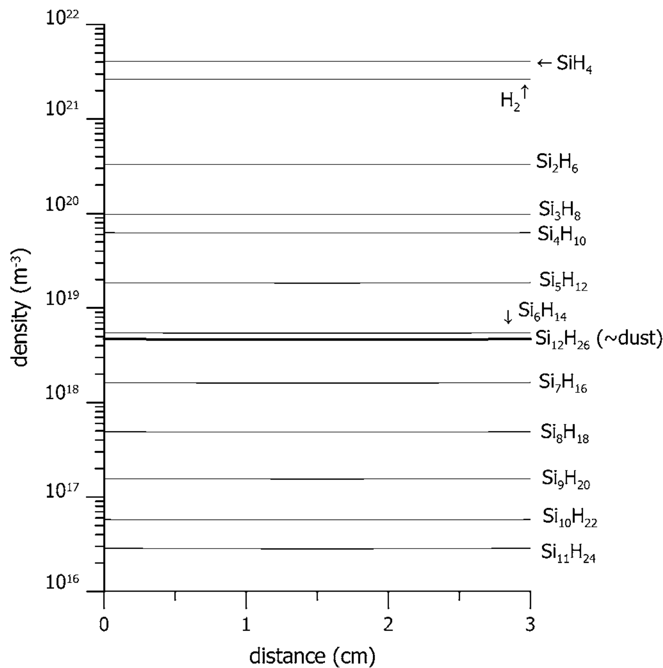

Fig. 2. Density profiles of silicon hydride molecules at a pressure of 0.3 torr, 5 W, 50 MHz, and 20 sccm inlet silane.

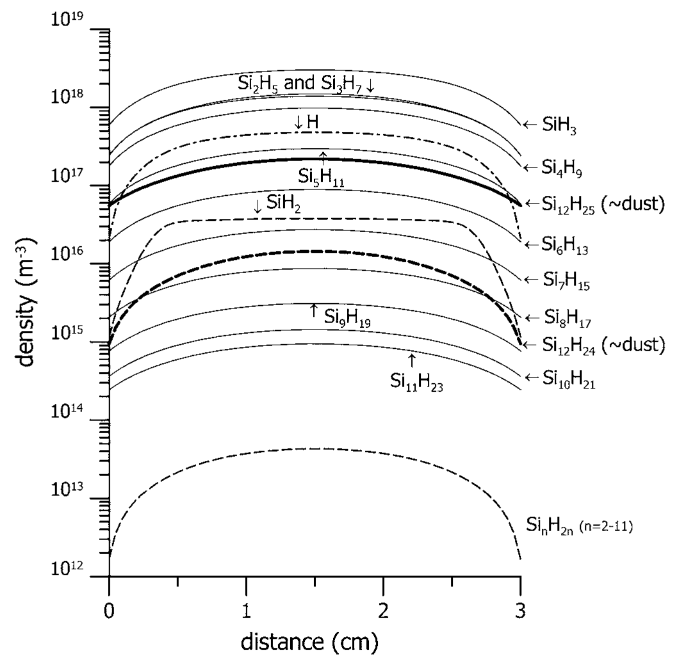

Fig. 3. Density profiles of the various silicon hydride radicals at a pressure of 0.3 torr, 5 W, 50 MHz, and 20 sccm inlet silane.

formed are $Si_{12}H_{25}^-$ and $Si_{12}H_{24}^-$. Indeed, these anions, in the figure also denoted as dust, have a density about two orders of magnitude higher than the other anions, because they are not lost due to the formation of bigger anions. Only the neutralization reactions with SiH_3^+ and $Si_2H_4^+$ provide a possible loss. These two species can thus be considered as the sum of all bigger negative ions. This also implies that $n_{SiH_3^+} + n_{Si_2H_4^+} \cong n_{e^-} + n_{Si_{12}H_{25}^-} + n_{Si_{12}H_{24}^-}$, where n denotes the number densities in the bulk plasma. The electron density is found to be in the order of 5×10^{14} m^{-3}.

The density profiles of the silyl and silylene anions exhibit peaks close to the sheath boundaries. This decrease in density in the plasma bulk is probably due to the fast anion-cation neutralization, which will mainly occur in the center of the discharge, where the density profiles of the positive ions reach a local maximum. As n increases, the peaks of the silyl and silylene density profiles tend to shift more inwards, possibly due to the reduced neutralization reaction rate and anion-neutral reaction rate, as explained above. Hence, the $Si_{12}H_{25}^-$ and $Si_{12}H_{24}^-$ density profiles do not reveal this specific shape, since they represent the sum of the density profiles of all bigger anions, which exhibit a maximum more and more to the center of the discharge.

It is clear from Fig. 1 that the silyl anion pathway (starting from SiH_3^-) is much more important in comparison with the silylene anion pathway. Indeed, the densities of silyl anions ($Si_nH_{2n+1}^-$) are one order of magnitude higher than those of silylene anions ($Si_nH_{2n}^-$), meaning that about 90% of the dust formation proceeds through the silyl anion pathway and only 10% through the silylene anion pathway.

In Fig. 2, the densities of the most important molecules (SiH_4, H_2, and Si_nH_{2n+2} with $n > 1$) are represented. The densities of the molecules are homogeneously distributed throughout the entire reactor and these species have much higher densities than the radicals, e.g., SiH_3 (see Fig. 3), which do undergo reactions at the electrodes. The densities of SiH_4, H_2, and Si_2H_6 are at least one order of magnitude higher than other neutral molecules and are commonly referred to as background neutrals. The inlet gas SiH_4 is present at the highest density (about 4×10^{21} m^{-3}), but also H_2 has a rather high density of almost 3×10^{21} m^{-3}. This is due to the fact that in many of the chemical reactions shown in Table III, molecular hydrogen is formed as a side product (e.g., reactions 1, 2, 4, 10, and 11). The higher order silanes, especially Si_2H_6, can, however, not be neglected either. Finally, note that, similar to Fig. 1, the density of the largest neutral species, $Si_{12}H_{26}$, is higher than would have been expected from the trend in decreasing density for higher molecules. This is due to the SiH_2 insertion reactions, which are stopped at $Si_{12}H_{26}$. Hence, again, $Si_{12}H_{26}$ stands for all higher order silanes.

In Fig. 3, the density profiles of the various radical species are shown. The radicals show a decreasing density toward the electrodes, representing their reactivity at the surface. The Si_nH_{2n+1} radicals (with $n = 1$ to 12), related to the silyl anions, are represented with a solid line, so that they are distinguished from the silylenes (Si_nH_{2n}, with $n = 1$ to 12), represented by a dashed line. The most important radical in the silane discharge is SiH_3 with a density of about 3×10^{18} m^{-3} in the center of the discharge. Again, the densities of $Si_{12}H_{25}$ and $Si_{12}H_{24}$ stand for a summation of the densities of all higher radicals. For reasons of clarity, the concentrations of all silylenes containing two to eleven silicon atoms are represented by a single line, since these species reach approximately the same concentration (due to the fact that the neutralization of silylene anions proceeds at almost the same reaction rate and it represents their only production process). As can been seen from Fig. 3, the silylenes have a relatively low density and thus are not considered to be important in our simulations. They

are only included since their respective anions form a possible clustering pathway.

IV. Conclusion

In this paper, we have used a one-dimensional fluid model to simulate cluster generation in silane plasmas and we have mainly focused our attention on particle nucleation and further growth. A total of 111 reactions among 65 silicon hydrides containing up to 12 silicon atoms were included in this model. Density profiles for the most important species were presented as a function of distance from the electrodes.

The anions play an indispensable role in the polymerization process, as negative ion-silane reactions represent the main pathway of particle growth. SiH_3^-, produced by dissociative electron attachment, forms the main starting point of anion formation and can be considered as the most important precursor of the dust formation. SiH_2^-, although less important, leads to the formation of silylenes anions ($Si_nH_{2n}^-$). The silyl anion pathway, starting from SiH_3^- and leading to the formation of $Si_nH_{2n+1}^-$ species, is much more important in comparison with the silylene anion pathway. It follows from our model that about 90% of the dust formation proceeds through the silyl anion pathway and only 10% through the silylene anion pathway.

In the future, this model will form the starting point for nanoparticle formation, and as the particles increase in size, coagulation of the clusters will be added.

Acknowledgment

The authors whish to thank Dr. U. V. Bhandarkar for the fitted kinetic parameters needed to calculate the various thermodynamical constants and for all the helpful discussions.

References

[1] J. Perrin, C. Böhm, R. Etemadi, and A. Lloret, “Possible routes for cluster growth and particle formation in RF silane discharges,” *Plasma Sources Sci. Technol.*, vol. 3, no. 3, pp. 252–261, 1994.

[2] A. Gallagher, “Model of particle growth in silane discharges,” *Phys. Rev. E*, vol. 62, no. 2, pp. 2690–2706, 2000.

[3] W. W. Stoffels and E. Stoffels, “Physics and application of dusty low pressure plasmas,” *Trends Vac. Sci. Technol.*, vol. 4, no. 1, pp. 1–35, 2001.

[4] J. Perrin and Ch. Hollenstein, “Sources and growth of particles,” in *Dusty Plasmas: Physics, Chemistry and Technological Impacts in Plasma Processing*, A. Bouchoule, Ed, Chichester, U.K.: Wiley, 1999, pp. 77–180.

[5] A. Bouchoule, A. Plain, L. Boufendi, J. Ph. Blondeau, and C. Laure, “Particle generation and behavior in a silane-argon low-pressure discharge under continuous or pulsed radio-frequency excitation,” *J. Appl. Phys.*, vol. 70, no. 4, pp. 1991–2000, 1991.

[6] G. S. Selwyn, J. Singh, and R. S. Benett, “In situ laser diagnostic studies of plasma-generated particulate contamination,” *J. Vac. Sci. Technol. A*, vol. 7, no. 4, pp. 2758–2765, 1989.

[7] C. Longeaud, J. P. Kleider, P. Roca i Cabarrocas, S. Hamma, R. Meaudre, and C. Meaudre, “Properties of a new a-Si:H-like material: Hydrogenated polymorphous silicon,” *J. Non-Cryst. Solids*, vol. 227–230, no. 1, pp. 96–99, 1998.

[8] M. Meaudre, R. Meaudre, R. Butté, and S. Vignoli, “Midgap density of states in hydrogenated polymorphous silicon,” *J. Appl. Phys.*, vol. 86, no. 2, pp. 946–950, 1999.

[9] L. Boufendi, W. Stoffels, and E. Stoffels, “Diagnostics of a dusty plasma,” in *Dusty Plasmas: Physics, Chemistry and Technological Impacts in Plasma Processing*, A. Bouchoule, Ed, Chichester, UK: Wiley, 1999, pp. 181–303.

[10] L. Boufendi and A. Bouchoule, “Particle nucleation and growth in a low-pressure argon-silane discharge,” *Plasma Sources Sci. Technol.*, vol. 3, no. 3, pp. 262–267, 1994.

[11] Ch. Hollenstein, J.-L. Dorier, J. Dutta, L. Sansonnens, and A. A. Howling, “Diagnostics of particle genesis and growth in RF silane plasmas by ion mass spectrometry and light scattering,” *Plasma Sources Sci. Technol.*, vol. 3, no. 3, pp. 278–285, 1994.

[12] A. A. Howling, L. Sansonnens, J.-L. Dorrier, and Ch. Hollenstein, “Negative hydrogenated silicon ion clusters as particle precursors in RF silane plasma deposition experiments,” *J. Phys. D, Appl. Phys.*, vol. 26, no. 6, pp. 1003–1007, 1993.

[13] S. J. Choi and M. J. Kushner, “The role of negative ions in the formation of particles in low-pressure plasmas,” *J. Appl. Phys.*, vol. 74, no. 2, pp. 853–861, 1993.

[14] G. J. Nienhuis, W. J. Goedheer, E. A. G. Hamers, W. G. J. H. M. van Sark, and J. Bezemer, “A self-consistent fluid model for radio-frequency discharges in SiH_4-H_2 compared to experiments,” *J. Appl. Phys.*, vol. 82, no. 5, pp. 2060–2071, 1997.

[15] G. J. Nienhuis, “Plasma models for silicon deposition,” Ph.D. dissertation, Utrecht University, 1998.

[16] D. L. Sharfetter and H. K. Gummel, “Large-signal analysis of a silicon read diode oscillator,” *IEEE Trans. Electron Devices*, vol. ED-16, p. 64, 1967.

[17] J. D. P. Passchier and W. J. Goedheer, “A two-dimensional fluid model for an argon rf discharge,” *J. Appl. Phys.*, vol. 74, no. 6, pp. 3744–3751, 1993.

[18] J. D. P. Passchier, “Numerical fluid models for RF discharges,” Ph.D. dissertation, Utrecht University, 1994.

[19] Ph. Belenguer and J. P. Boeuf, “Transition between different regimes of rf glow discharges,” *Phys. Rev. A*, vol. 41, no. 8, pp. 4447–4459, 1990.

[20] M. Surendra and D. B. Graves, “Particle simulations of radio-frequency glow discharges,” *IEEE Trans. Plasma Sci.*, vol. 19, pp. 144–157, Apr. 1991.

[21] Ch. Hollenstein, “The physics and chemistry of dusty plasmas,” *Plasma Phys. Control. Fusion*, vol. 42, no. 10, pp. R93–R104, 2000.

[22] E. Krishnakumar and S. K. Srivastava, “Ionization cross sections of silane and disilane by electron impact,” *Contrib. Plasma Phys.*, vol. 35, no. 4–5, pp. 395–404, 1995.

[23] M. Kurachi and Y. Nakamura, “Electron collision cross sections for the monosilane molecule,” *J. Phys. D, Appl. Phys.*, vol. 22, no. 1, pp. 107–112, 1989.

[24] J. Perrin, J. P. M. Schmitt, G. de Rosny, B. Drevillon, J. Huc, and A. Lloret, “Dissociation cross sections of silane and disilane by electron impact,” *Chem. Phys.*, vol. 73, no. 3, pp. 383–394, 1982.

[25] J. R. Doyle, D. A. Doughty, and A. Gallagher, “Silane dissociation products in deposition discharges,” *J. Appl. Phys.*, vol. 68, no. 9, pp. 4375–4384, 1990.

[26] P. Haaland, “Dissociative attachment in silane,” *J. Chem. Phys.*, vol. 93, no. 6, pp. 4066–4072, 1990.

[27] H. Tawara and T. Kato, “Total and partial ionization cross sections of atoms and ions by electron impact,” *At. Data Nucl. Data Tables*, vol. 36, no. 1, pp. 167–178, 1987.

[28] H. Ehrhardt, L. Langhans, F. Linder, and H. S. Taylor, “Resonance scattering of slow electrons from H_2 and CO angular distributions,” *Phys. Rev.*, vol. 173, no. 1, pp. 222–230, 1968.

[29] A. G. Engelhardt and A. V. Phelps, “Elastic and inelastic collision cross sections in hydrogen and deuterium from transport coefficients,” *Phys. Rev.*, vol. 131, no. 5, pp. 2115–2128, 1963.

[30] E. Krishnakumar and S. K. Srivastava, “Dissociative attachment of electrons with Si_2H_6,” *Int. J. Mass Spectrom. Ion. Processes*, vol. 103, no. 2–3, pp. 107–115, 1990.

[31] J. M. Wadehra and J. N. Bardsley, “Vibrational- and rotational-state dependence of dissociative attachment in e-H_2 collisions,” *Phys. Rev. Lett.*, vol. 41, no. 26, pp. 1795–1798, 1978.

[32] A. A. Fridman, L. Boufendi, T. Hbid, B. V. Potapkin, and A. Bouchoule, “Dusty plasma formation: Physics and critical phenomena. Theoretical approach,” *J. Appl. Phys.*, vol. 79, no. 3, pp. 1303–1314, 1996.

[33] U. V. Bhandarkar, M. T. Swihart, S. L. Girshick, and U. R. Kortshagen, “Modeling of silicon hydride clustering in a low-pressure silane plasma,” *J. Phys. D, Appl. Phys.*, vol. 33, no. 21, pp. 2731–2746, 2000.

[34] M. T. Swihart and S. L. Girshick, “Thermochemistry and kinetics of silicon hydride cluster formation during thermal decomposition of silane,” *J. Phys. Chem. B*, vol. 103, no. 1, pp. 64–76, 1999.

[35] ——, “Ab initio structures and energetics of selected hydrogenated silicon clusters containing six to ten silicon atoms,” *Chem. Phys. Lett.*, vol. 307, no. 5–6, pp. 527–532, 1999.

[36] J. Perrin, O. Leroy, and M. C. Bordage, "Cross-sections, rate constants and transport coefficients in silane plasma chemistry," *Contrib. Plasma Phys.*, vol. 36, no. 1, pp. 3–49, 1996.

[37] E. R. Austin and F. W. Lampe, "Rate constants for the reactions of hydrogen atoms with some silanes and germanes," *J. Phys. Chem.*, vol. 81, no. 12, pp. 1134–1138, 1977.

[38] N. Itabashi, K. Kato, N. Nishiwaki, T. Goto, C. Yamada, and E. Hirota, "Diffusion coefficient and reaction rate constant of the SiH_3 radical in silane plasma," *Jpn. J. Appl. Phys.*, vol. 28, pp. L325–L328, 1989.

[39] A. P. Hickman, "Approximate scaling formula for ion-ion mutual neutralization rates," *J. Chem. Phys.*, vol. 70, no. 11, pp. 4872–4878, 1979.

[40] U. V. Bhandarkar, private communication.

[41] U. Bhandarkar, U. Kortshagen, and S. L. Girshick, "Numerical study of the effect of gas temperature on the time for onset of particle nucleation in argon-silane low-pressure plasmas," *J. Phys. D, Appl. Phys.*, vol. 36, no. 12, pp. 1399–1408, 2003.

Kathleen De Bleecker was born in 1979. She received the M.Sc. degree in chemistry from the University of Antwerp, Wilrijk, Belgium, in 2002. She is currently pursuing the Ph.D. degree in sciences at the University of Antwerp.

Her research mainly focuses on the formation and behavior of nanoparticles in silane plasmas and is performed under the guidance of W. Goedheer and A. Bogaerts.

Annemie Bogaerts was born in 1971. She received the M.Sc. degree in chemistry and the Ph.D. degree in sciences from the University of Antwerp, Wilrijk, Belgium, in 1993 and 1996, respectively.

She has been a Professor of physical chemistry at the University of Antwerp since 2003. Her research interests include the modeling of glow discharges and related plasmas, plasma solids, ion solids, and laser solid interaction.

Wim Goedheer was born in The Netherlands in 1950. He received the physics and Ph.D. degrees from the University of Utrecht, Utrecht, The Netherlands, in 1973 and 1978, respectively.

Since 1973, he has been with the FOM-Institute for Plasma Physics, Nieuwegein, The Netherlands, where he has been mainly involved in modeling of partially ionized plasma, both in the boundary layers of a Tokamak and in industrial applications, including dusty and colloidal plasmas in capacitively coupled RF discharges.

Renaat Gijbels has been Professor of physical chemistry at the University of Antwerp, Wilrijk, Belgium, since 1973. His research interests include various types of inorganic mass spectrometry for bulk, surface and/or microanalysis, e.g., spark, laser ionization, and secondary ion and glow discharge mass spectrometry.